

Multi-pass quartz-enhanced photoacoustic spectroscopy-based trace gas sensing

SHUNDA QIAO,¹ YUFEI MA,^{1,*}  PIETRO PATIMISCO,² ANGELO SAMPAOLO,² YING HE,¹ ZITING LANG,¹ FRANK K. TITTEL,³ AND VINCENZO SPAGNOLO² 

¹National Key Laboratory of Science and Technology on Tunable Laser, Harbin Institute of Technology, Harbin 150001, China

²PolySense Lab–Dipartimento Interateneo di Fisica, University and Politecnico of Bari, Via Amendola 173, Bari, Italy

³Department of Electrical and Computer Engineering, Rice University, 6100 Main Street, Houston, Texas 77005, USA

*Corresponding author: mayufei@hit.edu.cn

Received 28 December 2020; revised 20 January 2021; accepted 23 January 2021; posted 26 January 2021 (Doc. ID 418520); published 17 February 2021

A multi-pass quartz-enhanced photoacoustic spectroscopy (MP-QEPAS)-based trace gas sensor is reported. In MP-QEPAS, a multi-pass laser beam pattern through the prong spacing of a quartz tuning fork (QTF) is obtained by means of two right-angle prisms. A large QTF with the prong length of 17 mm and prong spacing of 0.8 mm was employed to increase the passage of multi-pass time and ease the alignment of the beam reflection pattern through the QTF. This multi-pass configuration allows the laser beam to pass through the QTF prong spacing six times. Water vapor (H₂O) was chosen as target gas to investigate the performance of the MP-QEPAS sensor. Compared to a conventional QEPAS measurement, the MP-QEPAS technique provided an enhancement of signal level of ~3.2 times. © 2021 Optical Society of America

<https://doi.org/10.1364/OL.418520>

Trace gas detection methods based on laser absorption spectroscopy gained growing attention over the past years due to their merits of high sensitivity, excellent selectivity and fast response time [1–3]. They are widely used in various fields, such as medical diagnosis [4,5], combustion study [6], and industrial process monitoring [7]. Among the spectroscopic approaches, quartz-enhanced photoacoustic spectroscopy (QEPAS), exploiting a quartz tuning fork (QTF) as an acoustic wave transducer, is one of the most attractive techniques [8–11]. The light beam is focused between the QTF prongs, close to the antinode point of the flexural resonance mode, namely where the maximum deflection occurs. The high-quality factor and narrow resonance frequency of QTFs contribute in improving the sound-to-piezo current transduction efficiency and make the sensing system immune to environmental noise [12,13]. Furthermore, due to the reduced size and low cost of the sensitive element, QEPAS sensors are capable of combining compactness, ruggedness and cost affordability compared to other spectroscopic techniques [14–16], in which the optical detector represents an added major cost and space occupation.

The performance of a QEPAS sensor depends on the sound wave intensity generated by the absorbing gas that can be

enhanced by adopting high-power lasers [17–19] and by acoustically coupling the QTF with a pair of cylindrical metallic tubes that act as acoustic resonators [20–24]. However, an increase of performance can be also obtained by enhancing the light–gas interaction. Borri *et al.* reported an intracavity QEPAS sensor [25], where a standard 32.7 kHz QTF was inserted within a high-finesse, single-mode bow-tie optical cavity. The intracavity optical standing waves result in a resonant enhancement of the power of circulating light. An optical power buildup of ~320 has been reached in the infrared spectral range. Although the performance is highly improved, the use of optical cavities results in the loss of the compactness that usually distinguishes the QEPAS technique. In addition, the optical alignment, as well as the mode matching between the laser mode and one of cavity modes, is critical [26], making the sensor system poorly rugged and highly sensitive to mechanical instabilities, compromising its long-time stability. Zheng *et al.* presented a double antinode excited quartz-enhanced photoacoustic spectrophone (DAE-QEPAS) [27]. In this configuration, the QTF operates at the first overtone flexural mode, and an aluminum mirror and optical circulator were used to excite simultaneously both antinode points. A piezoelectric transducer was necessary to compensate for the phase shift between the two QTF antinodes that oscillates in anti-phase. The signal of the DAE-QEPAS sensor was improved ~3 times compared to a standard QEPAS spectrophone. However, the critical optical alignment with two antinode points, as well as high optical loss and phase sensitivity, significantly limit the ultimate performance. Complementary to optical cavities, multi-pass optical gas cells are used to multiply the light–gas interaction length exploiting reflections on multiple points on the mirrors composing the cell, which is usually adopted in tunable diode laser absorption spectroscopy [28].

The combination of the multi-pass approach with QEPAS must require that all reflected beams pass between prongs of the QTF. In this configuration, each light beam generates a point sound source between prongs that contributes to their deflection with a certain weight. In a first approximation, the weight can be supposed to be inversely proportional to the distance of the point sound source to the top of the prong. Thus, custom

QTFs, those with both long prongs and large prong spacing, are mandatory for an easy setup and optical alignment.

In this Letter, we report a multi-pass quartz-enhanced photoacoustic spectroscopy (MP-QEPAS)-based trace gas sensor. We used a large QTF with a prong length and width of 17 and 1 mm, respectively, resulting in a resonance frequency of 2.8 kHz for the fundamental mode. The spacing between the two prongs of the QTF is 0.8 mm. The QTF was placed inside a multi-pass optical system consisting of two right-angle prisms to make the laser beam pass through the QTF prong gap six times. The pair of prisms does not need a precise angle control, which makes the alignment easily. The fundamental resonance mode of the QTF was excited at different points: all local excitation points contribute to in-phase prong deflections, not requiring a phase shift compensator as was required for the overtone flexural mode of the DAE-QEPAS sensor. Water vapor (H_2O) was chosen as target analyte to investigate the performance of the MP-QEPAS sensor.

A schematic of the MP-QEPAS sensor system is depicted in Fig. 1. The laser source employed in this system is a tunable continuous-wave (CW) distributed feedback (DFB) diode laser emitting at 1395 nm. The laser power was 17 mW with the operating temperature of 22.5°C and driving current of 76 mA. The laser was first collimated by means of a fiber collimator (FC, Thorlabs, Model No. 50-1310A-APC) with a 0.25° divergence angle and then injected into the multi-pass system composed of a pair of right-angle prisms. The horizontal distance of the pair of right-angle prisms is 6 mm. The prisms are made of BK7 glass with a transmission as high as 91.6% at 1395 nm. The side lengths of the two prisms are 14 and 20 mm, respectively. In most of the QEPAS sensor systems demonstrated from 2002 to date, commercially available standard QTFs with a resonance frequency of 32.76 kHz are employed. The prongs are 3.9 mm

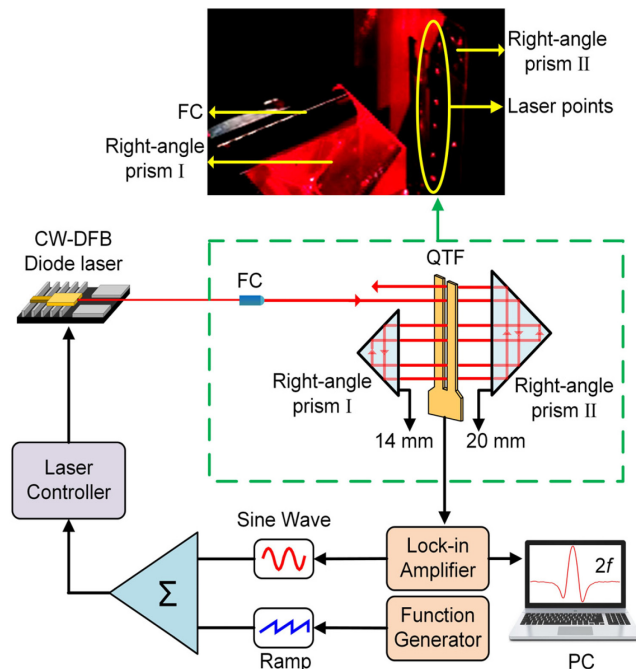


Fig. 1. MP-QEPAS system configuration. The laser passed through the gap of the QTF six times. CW-DFB, continuous-wave distributed feedback; FC, fiber collimator; QTF, quartz tuning fork; PC, personal computer.

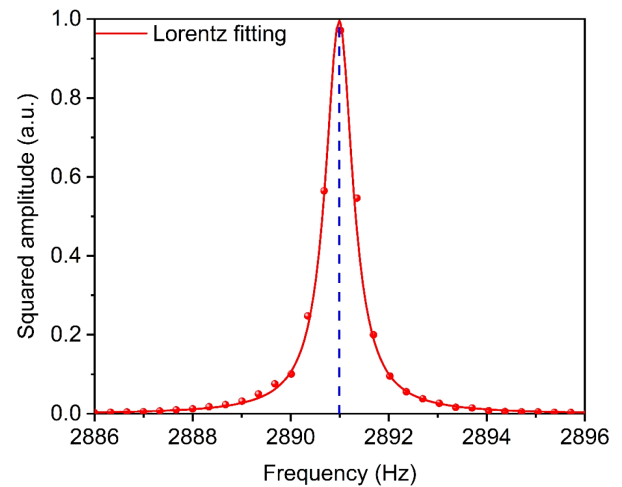


Fig. 2. Frequency response of the QTF. The data were normalized and fitted with a Lorentz function.

long, and the prong spacing is $\sim 300 \mu\text{m}$ [29]. These geometrical characteristics make a potential configuration based on multiple passes of the laser beam across different vertical points on the QTF axis unfeasible. With the aim of implementing a multi-pass configuration, a large, custom QTF was employed in the experimental setup [30]. The prongs of the custom QTF are 17 mm long, and the prong spacing is $800 \mu\text{m}$. The optical path was adjusted with the visible red laser light at first. By adjusting the relative height of two prisms, a six-time passage of laser beam was achieved. In the top of Fig. 1, six laser points on the front surface of the right-angle prism II are shown. In order to improve the performance of the MP-QEPAS sensor, wavelength modulation spectroscopy combined with 2nd-harmonic ($2f$) demodulation were implemented. A function generator was employed to provide a ramp wave with frequency of 10 mHz to the diode current for linearly scanning the laser wavelength across the target gas absorption line. The internal oscillator of the lock-in amplifier was used to generate a sine wave, which was used to modulate the laser wavelength at the half of the QTF resonance frequency. Finally, the piezo current generated by the QTF was demodulated by a lock-in amplifier and monitored by a software interface on a laptop. The detection bandwidth of the lock-in amplifier was 390 mHz. A 1.04% H_2O in the air was employed as target gas. An H_2O absorption line identified through the HITRAN database and located at 7168.4 cm^{-1} was selected for testing the MP-QEPAS sensor [31].

First, the resonance curve of the custom QTF was acquired to determine the wavelength modulation frequency. The laser wavelength was locked at the absorption peak, and the modulation frequency f_{mod} was scanned across half of the expected QTF resonance frequency. In Fig. 2, the normalized $2f$ -QEPAS signal is plotted versus the demodulation frequency ($2f_{\text{mod}}$). A Lorentzian fitting was imposed to retrieve the resonance frequency f_0 and the full width at half-maximum of the resonance curve Δf . The f_0 results in 2891 Hz, while $\Delta f = 0.68 \text{ Hz}$, leading to a QTF quality factor at the atmospheric pressure of $f_0/\Delta f = 4245$. The laser modulation frequency was thus set at $f_0/2 = 1445 \text{ Hz}$.

Before assessing the performance of the MP-QEPAS prototype, a standard single-pass QEPAS configuration was initially set up in order to set the basis for the estimation of the signal

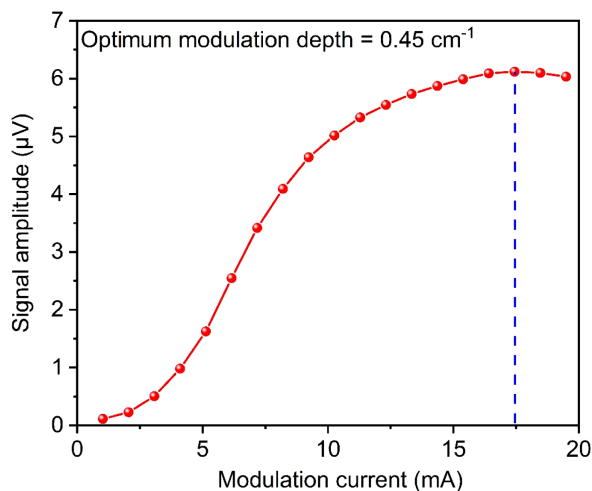


Fig. 3. Signal amplitude as a function of the current modulation depth. The optimal value was found to be 17.4 mA, corresponding to a wavelength modulation depth of 0.45 cm^{-1} .

enhancement. The setup was identical as depicted in Fig. 1 after removing the pair of right-angle prisms. The modulation depth of laser wavelength was varied to retrieve the highest QEPAS response. The measured signal amplitude as a function of the current modulation depth is shown in Fig. 3. The signal amplitude reaches its maximum with a current modulation depth of 17.4 mA, corresponding to a laser wavelength modulation depth of 0.45 cm^{-1} .

The vertical position of the laser spot [see Fig. 4(a)] for a single-pass QEPAS influences the prong deflection and, consequently, the piezo current generated [32]. In Fig. 4(b), the QEPAS signal was plotted at different vertical positions of the laser beam with respect to the top of the prongs (ΔL). The maximum QEPAS signal was recorded for $\Delta L = 1.5 \text{ mm}$, reaching a $2f$ -QEPAS signal peak of $6.11 \mu\text{V}$ at 200 ms of integration time. Note that the optimum laser beam position is not coincident with the antinode point of the resonance profile, corresponding to $\Delta L = 0$ in Fig. 4(b). This can be explained by considering that when the cylindrical-like spatial distribution of the acoustic source is at $\Delta L = 0$, a fraction of escape out the prong spacing; thus, it does not contribute to prong deflection. This decrease is in good agreement with the theoretical model proposed in Ref. [33].

Under the same experimental conditions, the performance of the MP-QEPAS sensor system was investigated by using the setup depicted in Fig. 1. The comparison between the $2f$ signal of the MP-QEPAS system and single-pass QEPAS configuration is shown in Fig. 5. The $2f$ -QEPAS signal peak for the MP-QEPAS was measured as $19.41 \mu\text{V}$, providing a ~ 3.2 signal enhancement compared to the maximum $2f$ -QEPAS signal peak of $6.11 \mu\text{V}$ obtained with single-pass configuration. Furthermore, the noise level of both systems was measured and found to be comparable. The QEPAS signal dependence on the vertical position of the laser spot justifies the nonlinear relation between the number of passes provided by the multi-reflection structure and the signal enhancement.

In conclusion, a gas sensor based on a multi-pass QEPAS approach, consisting of two right-angle prisms aligned with respect to a large QTF, has been demonstrated. A large QTF with the prong length of 17 mm and prong spacing of 0.8 mm

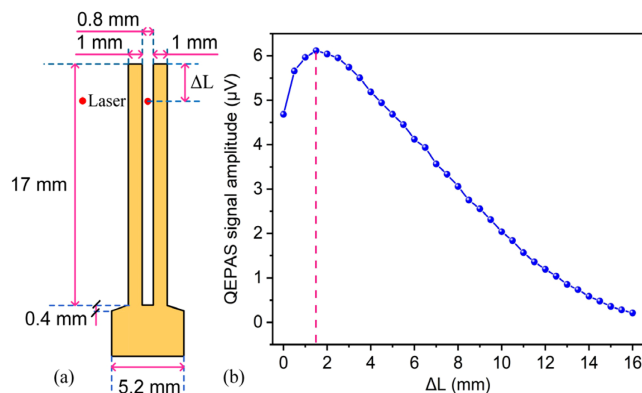


Fig. 4. (a) Vertical position of the laser spot with respect to the top of the prongs. (b) Signal amplitude as a function of ΔL .

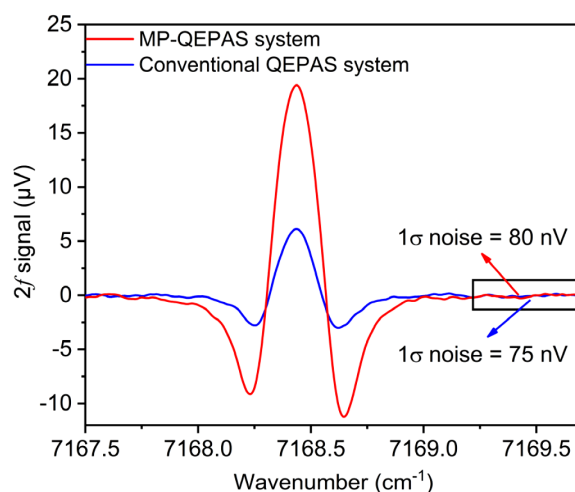


Fig. 5. $2f$ signal of the MP-QEPAS system (red line) and conventional standard QEPAS system (blue line), respectively.

was employed to increase the multi-pass time and ease the alignment of the beam reflection pattern through the QTF. This multi-reflection system permitted six passes of the laser through the prong gap of the QTF relying on a simple structure and easy alignment. Water vapor in the laboratory air was chosen as the target analyte to investigate the performance of the MP-QEPAS sensor. For comparison, a standard QEPAS configuration was also realized and tested. At the same conditions, the $2f$ signal amplitude of the MP-QEPAS system provided a ~ 3.2 times signal enhancement. The MP-QEPAS sensor performance can be further improved using prisms with higher reflectivity and by employing a pair of acoustic microresonator tubes at different vertical positions.

Funding. National Natural Science Foundation of China (61505041, 61875047, 62022032); Natural Science Foundation of Heilongjiang Province (YQ2019F006); Heilongjiang Provincial Postdoctoral Science Foundation (LBH-Q18052); Fundamental Research Funds for the Central Universities; THORLABS GmbH within the joint-research laboratory PolySense; Welch Foundation (C0586).

Disclosures. The authors declare no conflicts of interest.

REFERENCES

1. K. Krzempek, G. Dudzik, and K. Abramski, *Opt. Express* **26**, 28861 (2018).
2. H. D. Zheng, Y. H. Liu, H. Y. Lin, R. F. Kan, P. Patimisco, A. Sampaolo, M. Giglio, W. G. Zhu, J. H. Yu, F. K. Tittel, V. Spagnolo, and Z. Chen, *Opt. Express* **28**, 19446 (2020).
3. Y. F. Ma, Y. He, Y. Tong, X. Yu, and F. K. Tittel, *Opt. Express* **26**, 32103 (2018).
4. F. K. Tittel, R. Lewicki, L. Dong, K. Liu, T. H. Risby, S. Solga, and T. Schwartz, *Proc. SPIE* **8223**, 82230E (2012).
5. T. Milde, M. Hoppe, H. Tatenguem, M. Mordmüller, J. O'Gorman, U. Willer, W. Schade, and J. Sacher, *Appl. Opt.* **57**, C120 (2018).
6. J. E. Duque, S. López, and A. Molina, *Appl. Opt.* **57**, 6707 (2018).
7. P. Kluczynski, M. Jahjah, L. Nähle, O. Axner, S. Belahsene, M. Fischer, J. Koeth, Y. Rouillard, J. Westberg, A. Viect, and S. Lundqvist, *Appl. Phys. B* **105**, 427 (2011).
8. Y. F. Ma, *Appl. Sci.* **8**, 1822 (2018).
9. P. Patimisco, A. Sampaolo, L. Dong, F. K. Tittel, and V. Spagnolo, *Appl. Phys. Rev.* **5**, 011106 (2018).
10. H. M. Yi, R. Maamary, X. M. Gao, M. W. Sigrist, E. Fertein, and W. D. Chen, *Appl. Phys. Lett.* **106**, 101109 (2015).
11. L. G. Xu, N. W. Liu, S. Zhou, L. Zhang, B. L. Yu, H. Fischer, and J. S. Li, *Opt. Express* **28**, 5648 (2020).
12. Y. F. Ma, S. D. Qiao, P. Patimisco, A. Sampaolo, Y. Wang, F. K. Tittel, and V. Spagnolo, *Appl. Phys. Lett.* **116**, 061101 (2020).
13. Z. L. Li, Z. Wang, Y. Qi, W. Jin, and W. Ren, *Sens. Actuators, B* **248**, 1023 (2017).
14. Y. F. Ma, *Front. Phys.* **8**, 268 (2020).
15. J. P. Waclawek, H. Moser, and B. Lendl, *Opt. Express* **24**, 6559 (2016).
16. M. Mordmüller, M. Köhring, W. Schade, and U. Willer, *Appl. Phys. B* **119**, 111 (2015).
17. Y. F. Ma, R. Lewicki, M. Razeghi, and F. K. Tittel, *Opt. Express* **21**, 1008 (2013).
18. H. P. Wu, A. Sampaolo, L. Dong, P. Patimisco, X. L. Liu, H. D. Zheng, X. K. Yin, W. G. Ma, L. Zhang, W. B. Yin, V. Spagnolo, S. T. Jia, and F. K. Tittel, *Appl. Phys. Lett.* **107**, 111104 (2015).
19. Y. Li, R. Z. Wang, F. K. Tittel, and Y. F. Ma, *Opt. Lasers Eng.* **132**, 106155 (2020).
20. K. Liu, X. Y. Guo, H. M. Yi, W. D. Chen, W. J. Zhang, and X. M. Gao, *Opt. Lett.* **34**, 1594 (2009).
21. H. D. Zheng, L. Dong, A. Sampaolo, H. P. Wu, P. Patimisco, X. K. Yin, W. G. Ma, L. Zhang, W. B. Yin, V. Spagnolo, S. T. Jia, and F. K. Tittel, *Opt. Lett.* **41**, 978 (2016).
22. R. Rousseau, Z. Loghmani, M. Bahriz, K. Chamassi, R. Teissier, A. N. Baranov, and A. Vicet, *Opt. Express* **27**, 7435 (2019).
23. Y. F. Ma, Y. Tong, Y. He, X. G. Jin, and F. K. Tittel, *Opt. Express* **27**, 9302 (2019).
24. S. D. Russo, M. Giglio, A. Sampaolo, P. Patimisco, G. Menduni, H. P. Wu, L. Dong, V. M. N. Passaro, and V. Spagnolo, *Sensors* **19**, 4109 (2019).
25. S. Borri, P. Patimisco, I. Galli, D. Mazzotti, G. Giusfredi, N. Akikusa, M. Yamanishi, G. Scamarcio, P. De Natale, and V. Spagnolo, *Appl. Phys. Lett.* **104**, 091114 (2014).
26. P. Patimisco, A. Sampaolo, F. K. Tittel, and V. Spagnolo, *Sens. Actuators, A* **267**, 70 (2017).
27. H. D. Zheng, L. Dong, P. Patimisco, H. P. Wu, A. Sampaolo, X. K. Yin, S. Z. Li, W. G. Ma, L. Zhang, W. B. Yin, L. T. Xiao, V. Spagnolo, S. T. Jia, and F. K. Tittel, *Appl. Phys. Lett.* **110**, 021110 (2017).
28. R. Y. Cui, L. Dong, H. P. Wu, W. G. Ma, L. T. Xiao, S. T. Jia, W. D. Chen, and F. K. Tittel, *Anal. Chem.* **92**, 13034 (2020).
29. Y. F. Ma, Y. Q. Hu, S. D. Qiao, Y. He, and F. K. Tittel, *Photoacoustics* **20**, 100206 (2020).
30. P. Patimisco, A. Sampaolo, H. D. Zheng, L. Dong, F. K. Tittel, and V. Spagnolo, *Adv. Phys. X* **2**, 169 (2016).
31. I. E. Gordon, L. S. Rothman, C. Hill, R. V. Kochanov, Y. Tan, P. F. Bernath, M. Birk, V. Boudon, A. Campargue, K. V. Chance, B. J. Drouin, J. M. Flaud, R. R. Gamache, J. T. Hodges, D. Jacquemart, V. I. Perevalov, A. Perrin, K. P. Shine, M.-A. H. Smith, J. Tennyson, G. C. Toon, H. Tran, V. G. Tyuterev, A. Barbe, A. G. Császár, V. M. Devi, T. Furtenbacher, J. J. Harrison, J.-M. Hartmann, A. Jolly, T. J. Johnson, T. Karman, I. Kleiner, A. A. Kyuberis, J. Loos, O. M. Lyulin, S. T. Massie, S. N. Mikhailenko, N. Moazzen-Ahmadi, H. S. P. Müller, O. V. Naumenko, A. V. Nikitin, O. L. Polyansky, M. Rey, M. Rotger, S. W. Sharpe, K. Sung, E. Starikova, S. A. Tashkun, J. Auwera, J. V. Auwera, G. Wagner, J. Wilzewski, P. Wcisło, S. Yu, and E. J. Zak, *J. Quant. Spectrosc. Radiat. Transf.* **203**, 3 (2017).
32. Y. F. Ma, Y. He, L. G. Zhang, X. Yu, J. B. Zhang, R. Sun, and F. K. Tittel, *Appl. Phys. Lett.* **110**, 031107 (2017).
33. P. Patimisco, G. Scamarcio, F. K. Tittel, and V. Spagnolo, *Sensors* **14**, 6165 (2014).